Supporting information

Reducing Lattice Thermal Conductivity of MnTe by Se Alloying toward High Thermoelectric Performance

Jinfeng Dong[a], Fu-Hua Sun[a], Huaichao Tang[a], Kei Hayashi[b], Hezhang Li[b], Peng-Peng Shang[a,c], Yuzuru Miyazaki[b] and Jing-Feng Li[a]*

[a]State Key Laboratory of New Ceramics and Fine Processing, School of Materials Science and Engineering, Tsinghua University, Beijing, 100084, China.

[b]Departmant of Applied Physics, Graduate School of Engineering, Tohoku University, Sendai, 980-8579, Japan.

[c]College of Chemistry and Materials Science, Shandong Agricultural University, Taian, 271018, PR China.

* Corresponding authors. Emails: jingfeng@mail.tsinghua.edu.cn.

Phase and compositions of samples

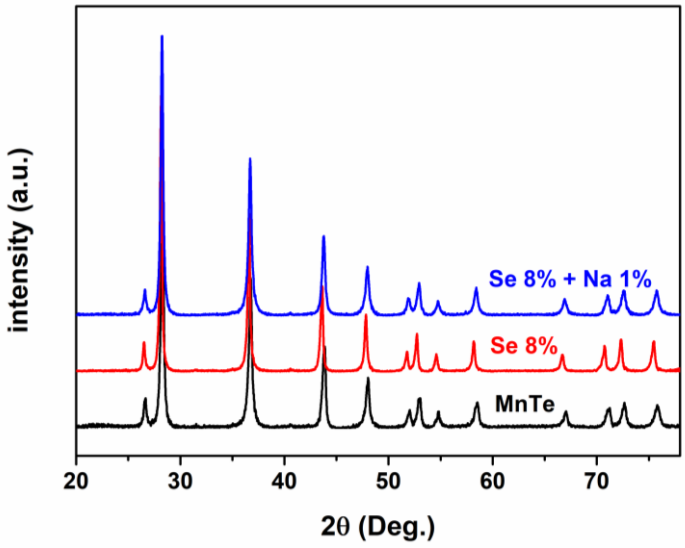

Figure S1. XRD pattern of Se alloyed and Na doped MnTe.

According to the XRD patterns shown in **Figure S1**, the rather high phase purity was confirmed in $MnTe_{0.92}Se_{0.08}$ and $Na_{0.01}Mn_{0.99}Te_{0.92}Se_{0.08}$.

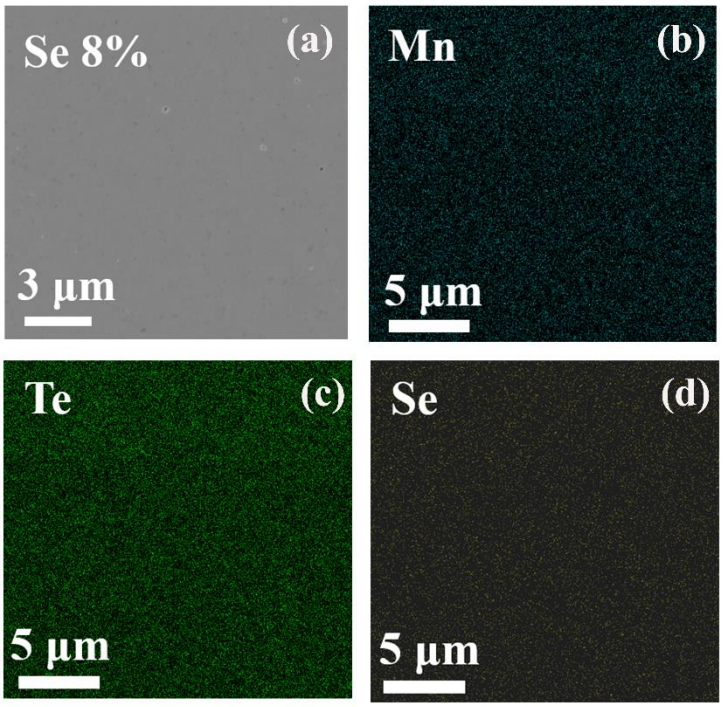

Figure S2. (a) SEM image on the polished surface of $MnTe_{0.92}Se_{0.08}$. EDS mapping of (b) Mn, (c) Te and (d) Se.

Figure S2a shows a uniform contract without secondary phase. The EDS mapping of Mn, Te and Se indicated that the elements are homogenously distributed in the matrix, confirming a high phase purity.

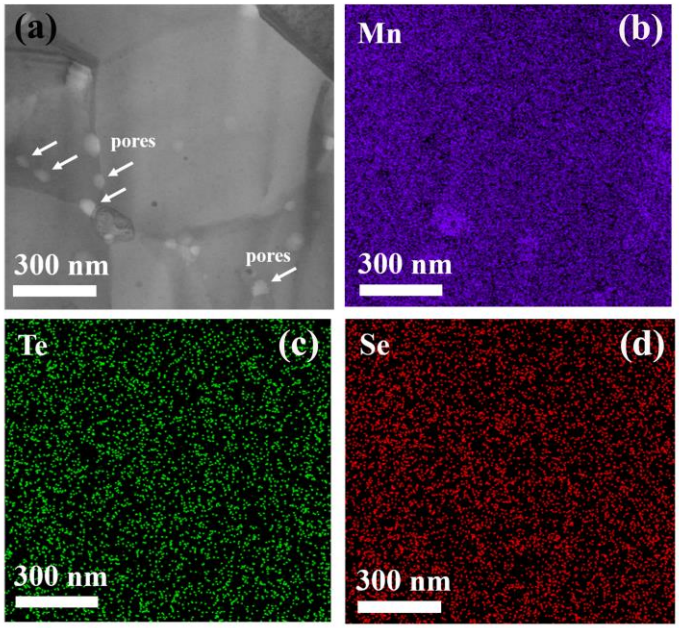

Figure S3. (a) The TEM image of $MnTe_{0.92}Se_{0.08}$ showing several grains. EDS mapping of (b) Mn, (c) Te and (d) Se.

Figure S3 confirms the homogeneity of elements (Mn, Te and Se) at a nanoscale, except for a little segregation of Mn in grain boundaries.

Hall measurement results and schematic illustration of band gap

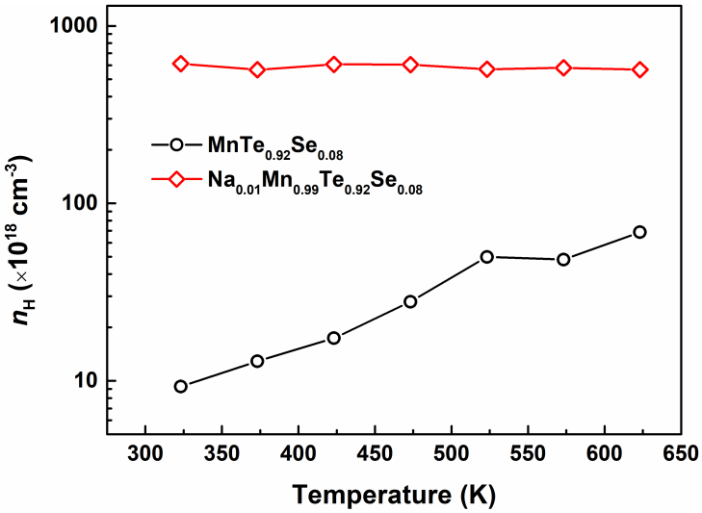

Figure S4 Temperature denpendent hole carrier concentration of $MnTe_{0.92}Se_{0.08}$ and $Na_{0.01}Mn_{0.99}Te_{0.92}Se_{0.08}$.

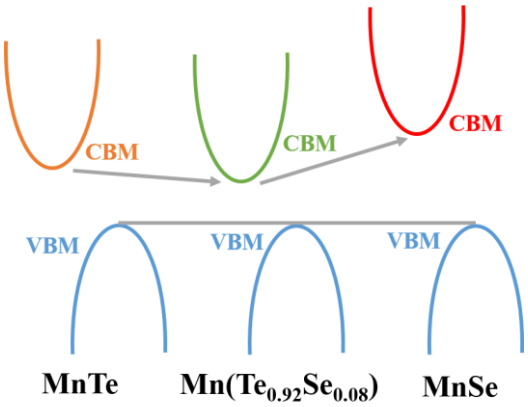

Figure S5 A simple schematic illustration represents the variation of the band gap

Thermal conductivity

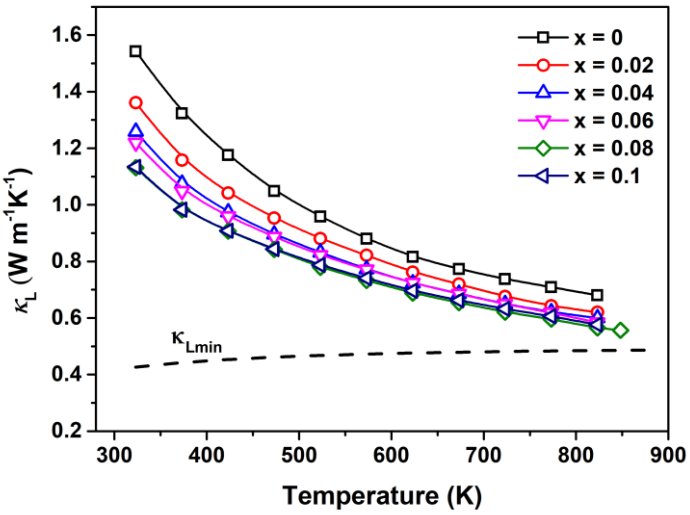

Figure S6 temperature-dependent lattice thermal conductivity of $MnTe_{1-x}Se_x$.

The uncorrected lattice thermal conductivity of $MnTe_{1-x}Se_x$ was shown in **Figure S4**. The lattice thermal conductivity monotonously decreases with the increase of Se contents. The low lattice thermal conductivity of $MnTe_{1-x}Se_x$ at 850 K is close to the amorphous limit.

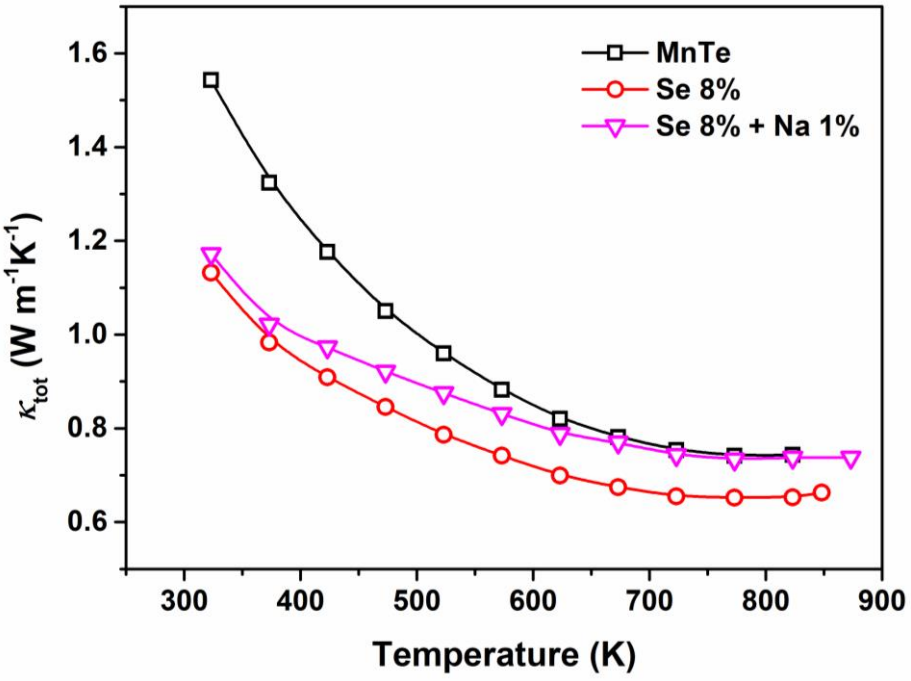

Figure S7. Temperature-dependent thermal conductivity of Se alloyed and Na doped MnTe.

The total thermal conductivity of Se alloyed and Na doped MnTe is shown in **Figure S5**, which shows an enhanced value compared to the Se alloyed samples. The increased thermal conductivity is ascribed to the increased electronic thermal conductivity.

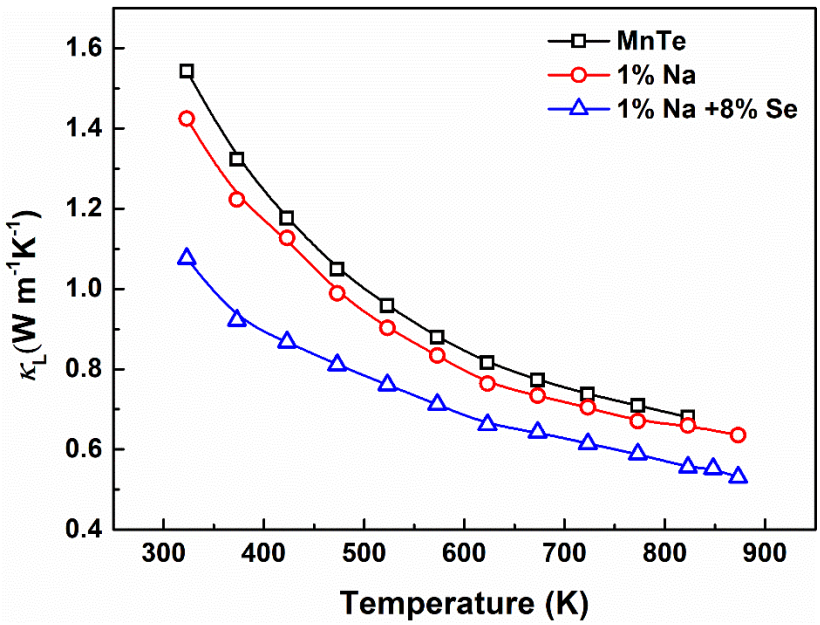

Figure S8. Temperature-dependent lattice thermal conductivity of Se alloyed and Na doped MnTe.

The lattice thermal conductivity of Se alloyed and Na doped MnTe is shown in **Figure S6**, which indicates that Se alloyed samples hold the lowest lattice thermal conductivity. The reduction of lattice thermal conductivity by Na doping is limited due to the low solubility of Na as the lattice thermal conductivity satuated even more Na was introduced[1]. So the high solubility of Se could provide sufficient scattering centers than Na, which guarantees the lowest lattice thermal conductivity.

Repeat measurements

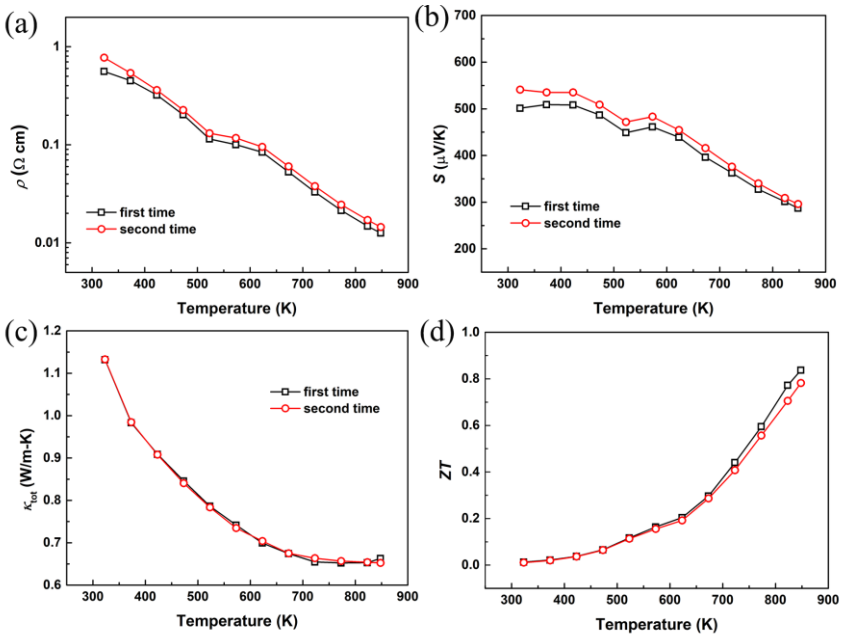

Figure S9. Repeat measurement results of (a) electrical resistivity, (b) Seebeck coefficient, (c) thermal conductivity and (d) *ZT* for $MnTe_{0.92}Se_{0.08}$.

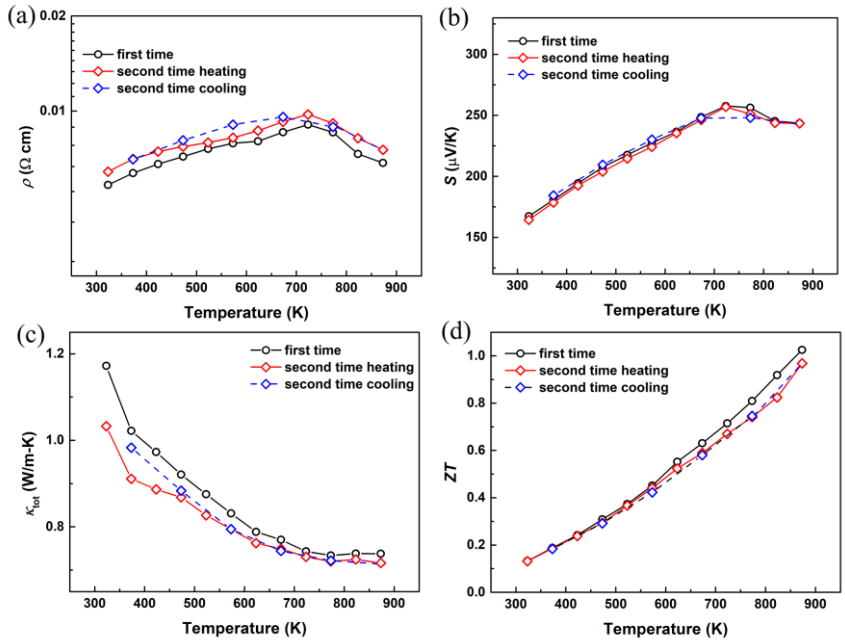

Figure S10. Repeat measurement results of (a) electrical resistivity, (b) Seebeck coefficient, (c) thermal conductivity and (d) *ZT* for $Na_{0.01}Mn_{0.99}Te_{0.92}Se_{0.08}$.

The repeat measurement of $MnTe_{0.92}Se_{0.08}$ and $Na_{0.01}Mn_{0.99}Te_{0.92}Se_{0.08}$ shows similar electrical and thermal transport properties, confirming the stability of samples.

Cycle measurement and DSC-TG test

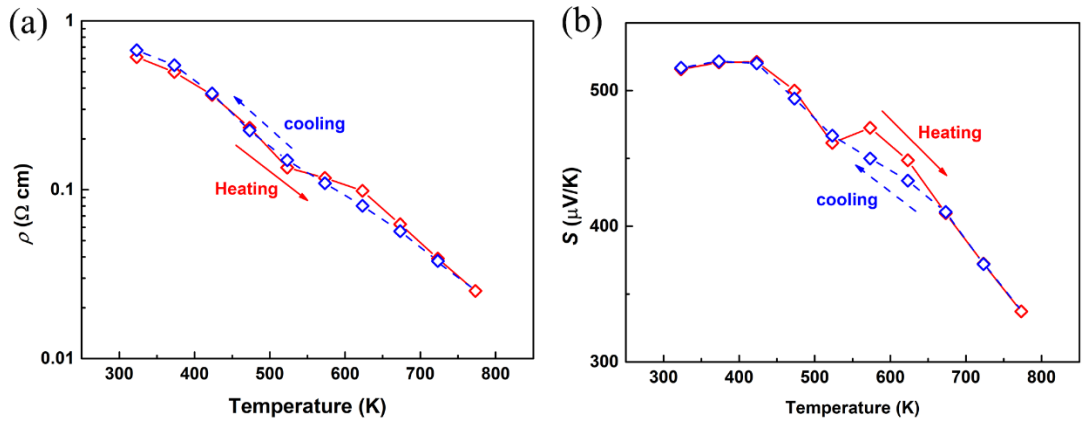

Figure S11. Heating and cooling measurement of (a) electrical resistivity, (b) Seebeck coefficient, for $MnTe_{0.92}Se_{0.08}$.

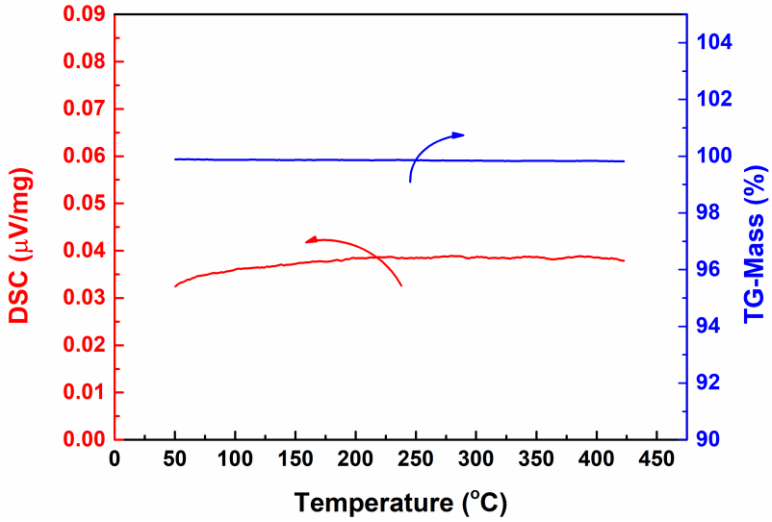

Figure S12. DSC and TG results of $MnTe_{0.92}Se_{0.08}$.

The abnormal inflection of electric resistivity and Seebeck coefficient at around 500 K for $MnTe_{0.92}Se_{0.08}$ have been reserved for the second measurement (**Figure S7**) and third measurement (**Figure S9**), when the measurement was conducted with the heating procedure. However, the measurement during the cooling procedure as shown in **Figure S9** doesnot show such an abnormal dip. Moreover, The smooth DSC signal also eliminate the possibility of phase transformation and the TG signal suggests no element evaporation. Thus, the abnormal inflection may be induced by some thermally activated defects.

Detailed calculation of Debye temperature and total relaxation time $\tau(x)$

In this work, Debye temperature was estimated to be 175 K *via*[2, 3]

$$\Theta = \frac{h}{k_B}[\frac{3N}{4\pi V}]^{1/3} v_a \quad (1)$$

where N is the number of atoms in the unit cell, V is the unit-cell volume and v_a is the average sound velocity.

The total relaxation time τ(x) could be derived from different scattering process including Umklapp, grain boundary and point defects scattering, while the influence of nano-pores is not taken into account for the correction of porosity and the same microstructure of pristine and Se alloyed MnTe. The expression of $\tau(x)$ was shown as Equation 1.

$$\tau^{-1}(x) = \tau_U{}^{-1}(x) + \tau_{GD}{}^{-1}(x) + \tau_{PD}{}^{-1}(x) \quad (2)$$

$\tau_U{}^{-1}(x)$ represents scattering frequency for Umklapp process and expressed as[4]

$$\tau_U{}^{-1}(x) = \frac{k_B{}^2\gamma^2}{\hbar M v_a{}^2 \theta_a} x^2 T^3 e^{-\theta_a/3T} \quad (3)$$

Where M is the average mass per atom, γ is the Grüneisen parameter that is determined by fitting the experimental data of pristine MnTe and a reasonable value of 2.5 is applied to yield the best simulation. $\tau_{GD}{}^{-1}(x)$ relates the average grain size (L) with scattering of phonons *via*

$$\tau_{GD}{}^{-1}(x) = v_a / L \quad (4)$$

As for the point defects scattering, the relaxation time $\tau_{PD}{}^{-1}(x)$ is estimated by[5]

$$\tau_{PD}{}^{-1}(x) = \frac{k_B{}^4 V_{atom} \Gamma}{4\pi\hbar^4 v_a{}^3} x^4 T^4 \quad (5)$$

Here, Γ is comprised of contributions from the mass (Γ_{mass}) and strain (Γ_{strain}) fluctuations induced by guest atoms, which are given by[5]

$$\Gamma_{mass} = n_{sublatt}(\frac{\overline{M_{sublatt}}}{M_{compd}})x(1-x)[\frac{M_1 - M_2}{\overline{M_{sublatt}}}]^2 / n_{compd} \quad (6)$$

$$\Gamma_{strain} = n_{sublatt}(\frac{\overline{M_{sublatt}}}{M_{compd}})x(1-x)\varepsilon[\frac{R_1 - R_2}{\overline{R_{sublatt}}}]^2 / n_{compd} \quad (7)$$

$n_{sublatt}$ and n_{compd} are the sublattice and total occupancy (Here for $MnTe_{1-x}Se_x$, $n_{sublatt}$ = 1 and n_{compd} = 2); $\overline{M_{sublatt}}$ and $\overline{R_{sublatt}}$ denote the average atomic mass and radius for the sublattice; M_i and R_i represent atomic mass and radius of atoms 1 and 2 (Te and

Se)[6], $\overline{M_{compd}}$ and ε are average atomic mass of $MnTe_{1-x}Se_x$ and strain field factor (It is simulated to be 45 in this work). All the parameters used in this work are listed in the following **table S1**

Table S1 Parameters for thermal transport modeling

Parameters	Average sound velocity, v_a (m s^{-1})	Debye temperature, Θ (K)	Grüneisen parameter, γ	Average grain size, L_a (μm)	strain field factor, ε
value	2170	175	2.5	1	45

Table S2 Dentisy of different samples

Composition of samples	Theoretical density	Pristine MnTe	2% Se	4% Se	6% Se	8% Se	10% Se	8% Se+1% Na
Density (g/cm^3)	6.02	5.88	5.94	5.92	5.88	5.88	5.87	5.84

References

(1). Dong, J.; Wu, C.-F.; Pei, J.; Sun, F.-H.; Pan, Y.; Zhang, B.-P.; Tang, H.; Li, J.-F., Lead-free MnTe Mid-Temperature Thermoelectric Materials: Facile Synthesis, P-type Doping and Transport Properties. J. Mater. Chem. C **2018,** 6 (15), 4265-4272.

(2). Xiao, Y.; Chang, C.; Pei, Y.; Wu, D.; Peng, K.; Zhou, X.; Gong, S.; He, J.; Zhang, Y.; Zeng, Z.; Zhao, L.-D., Origin of Low Thermal Conductivity in SnSe. *Phy. Rev. B* **2016,** 94 (12) 125203-125209, .

(3). Kurosaki, K.; Kosuga, A.; Muta, H.; Uno, M.; Yamanaka, S., Ag_9TlTe_5: A High-Performance Thermoelectric Bulk Material with Extremely Low Thermal Conductivity. Appl. Phys. Lett. **2005,** 87 (6), 061919-061921.

(4). Slack, G. A.; Galginaitis, S., Thermal Conductivity and Phonon Scattering by Magnetic Impurities in CdTe. Phy. Rev. **1964,** *133* (1A), A253-A268.

(5). Wan, C. L.; Pan, W.; Xu, Q.; Qin, Y. X.; Wang, J. D.; Qu, Z. X.; Fang, M. H., Effect of Point Defects on the Thermal Transport Properties of$(La_xGd_{1-x})_2Zr_2O_7$: Experiment and Theoretical Model. Phy. Rev. B **2006,** 74 (14) 144109-144118.

(6). Shannon, R. T.; Prewitt, C. T., Effective Ionic Radii in Oxides and Fluorides. Acta Crystallogr. Sect. B: Struct. Crystallogr. Cryst. Chem. **1969,** 25 (5), 925-946.